Elastoacoustic model with uncertain mechanical properties for ultrasonic wave velocity prediction; application to cortical bone evaluation

Karina Macocco[a)]

Laboratoire de Mécanique Physique, CNRS UMR 7052 B2OA
Faculté des Sciences et Technologie, Université Paris XII-Val de Marne
61, Avenue du Général de Gaulle, 94010 Créteil Cédex, FRANCE.

Quentin Grimal[b)]

Laboratoire d'Imagerie Paramétrique, CNRS UMR 7623
Université Pierre et Marie Curie
15, rue de l'école de médecine, 75006 Paris, FRANCE.

Salah Naili[c)]

Laboratoire de Mécanique Physique, CNRS UMR 7052 B2OA
Faculté des Sciences et Technologie, Université Paris XII-Val de Marne
61, avenue du Général de Gaulle, 94010 Créteil Cédex, FRANCE.

Christian Soize[d)]

Laboratoire de Mécanique,
Université de Marne la Vallée, 5 boulevard Descartes,
77454 Marne la Vallée Cédex 2, FRANCE.

(Dated: 22nd July 2005)

Running title: Elastoacoustic model

[a)] Electronic address: macocco@univ-paris12.fr
[b)] Electronic address: quentin.grimal@upmc.fr
[c)] Electronic address: naili@univ-paris12.fr
[d)] Electronic address: soize@univ-mlv.fr

Abstract

The axial transmission technique can measure the longitudinal wave velocity of an immersed solid. A model of the technique is developed with a set of source and receivers placed in a semi-infinite fluid coupled at a plane interface with a semi-infinite solid. The acoustic fluid is homogeneous. The solid is homogeneous, isotropic and linearly elastic. The work is focused on the prediction of the measured velocity (apparent velocity) when the solid is considered to have random material properties. The probability density functions of the random variables modeling each mechanical parameter of the solid are derived following the maximum entropy principle. Specific attention is paid to the modeling of Poisson's ratio so that the second-order moments of the velocities remain finite. The stochastic solver is based on a Monte Carlo numerical simulation and uses an exact semi-analytic expression of the acoustic response derived with the Cagniard-de Hoop method. Results are presented for a solid with the material properties of cortical bone. The estimated mean values and confidence regions of the apparent velocity are presented for various dispersion levels of the random parameters. A sensibility analysis with respect to the source and receivers locations is presented.

PACS numbers: 43.20.-f (General linear acoustics)

I. INTRODUCTION

This paper deals with predicting the reflection of a transient wave at a plane interface between a semi-infinite fluid and an semi-infinite solid in the ultrasonic range, when the source and receiver are placed in the fluid. This configuration is an elementary model of the "axial transmission" technique used to evaluate the mechanical properties of cortical bone (Bossy *et al.* (2004); Foldes *et al.* (1995); Lowet and Van der Perre (1996)). This technique may also be used for non-destructive evaluation of classical engineering materials. The technique uses the lateral wave (also known as "head wave") which propagates in the solid at the velocity of longitudinal waves, close to the interface, and is refracted in the fluid at the critical angle (Brekhovskikh (1960)). From the measurements of the times of flight associated with the lateral wave, the longitudinal wave velocity in the solid can be estimated; this estimation is referred to as the *apparent* velocity. In the context of bone evaluation, the solid and the fluid represent bone and soft tissues (skin, muscle), respectively. The purpose of such ultrasonic measurements of bones is to identify the individuals with excessive bone fragility and fracture risk associated with various pathologies.

In principle, it would be possible to estimate mechanical parameters of the solid from the measured elasto-acoustic response of the system which is built as the superposition of two semi-infinite media separated by a plane interface. This implies to solve an intricate inverse problem. This work, which presents the forward modeling of the elasto-acoustics response with several simplifying assumptions, is a first step toward the identification of the mechanical parameters with the axial transmission technique. This study should contribute to a better interpretation of measurements and help to develop new ultrasonic methods.

The novelty of this work is mainly to consider the solid with random material properties. The probabilistic framework is thought to be a good candidate to take into account intrinsic physiological variations of bone material properties. Indeed, bone can be viewed as a material with random properties because its effective macroscopic properties depend on many factors (genetic, environment, physiological, pathological), at various length scales.

The fluid parameters and the respective locations of the source and receivers are deterministic parameters in the problem.

The uncertainties of the solid material parameters are modeled by using the usual parametric approach, that is, each uncertain mechanical parameters is modeled by a random

variable. A particular attention is devoted to the probabilistic model of the random variable associated with the Poisson ratio in order that the longitudinal and transverse wave velocities have a finite second-order moment. The probability models of the uncertain parameters are then constructed by using the maximum entropy principle (Shannon (1948); Jaynes (1957a,b); Kapur and Kesavan (1992)). The maximum entropy principle is especially powerful to construct a probabilistic model of bone because available experimental data sets are usually not sufficiently large to estimate a probability density functions by using mathematical statistics. The expressions derived in this paper for the probability density function are *a priori* valid for all bones types and can be adapted to any specific set of bone samples (specific bone type, specific species, etc.) by providing a mean value.

Taking advantage of the simple configuration considered, an exact solution of the elasto-acoustics problem is used. This solution, corresponding to the reflection of a cylindrical wave on a semi-infinite solid, is obtained with the help of the Cagniard-de Hoop technique (Cagniard (1939); de Hoop (1960)). The solution is available in a semi-analytic form, namely closed-form analytic Green's function convolved with a function of the source history.

The final output of the method developed is the probability density function of the apparent velocity of longitudinal waves in the solid. It is calculated by using the probabilistic model associated with the elasto-acoustic equations. The stochastic solver is based on the Monte Carlo simulation method. Realizations of the random variables are obtained with generators adapted to the problem. The computational time is reasonable thanks to the use of the Cagniard-de Hoop solution.

The paper is organized as follows. The elasto-acoustic problem is formulated in Section II. In Section III, the procedure for calculating the apparent velocity is presented for the mean problem, that is, for the associated deterministic problem; the Cagniard-de Hoop solution for the elasto-acoustic response is given in this section. The probabilistic models associated with the three uncertain parameters are constructed in Section IV. Section V is devoted to the stochastic solver and to the estimation of the mean value, the variance and the probability distribution of the random solution (variable modeling the apparent velocity of longitudinal waves). The mean values of the solid material parameters used for the computations, obtained from the literature on cortical bone, are presented in Section VI. The analysis of the random solution is presented in Section VII for a set of cortical bone samples. Finally, Section VIII outlines a conclusion and the appendix deals with some of

the technical aspects in greater detail.

II. PROBLEM FORMULATION

A. Configuration and definitions

The geometry adopted is shown in Fig. 1. It consists in the superposition of two semi-infinite media separated by a plane interface. The upper medium is a homogeneous acoustic fluid; the lower one is a homogeneous, isotropic and linear elastic solid.

The position is specified through the Cartesian coordinates (x_1, x_2, x_3) with respect to a Cartesian reference frame $\mathbf{R}(O; \mathbf{x}_1, \mathbf{x}_2, \mathbf{x}_3)$ where O is the origin of the space and $(\mathbf{x}_1, \mathbf{x}_2, \mathbf{x}_3)$ is an orthonormal basis of this space. The x_3-axis is chosen downwards and normal to the fluid-solid interface. The fluid occupies the unbounded domain Ω_1 defined as the half-space $x_3 < 0$ and the solid the unbounded domain Ω_2 defined as the half-space $x_3 > 0$. The plane interface $\partial\Omega$ has the equation $x_3 = 0$.

Time coordinate is denoted by t. The fluid and the solid are at rest at times $t < 0$. At $t = 0$, a line source parallel to $(O; \mathbf{x}_2)$, placed in the fluid at a distance h_s from the interface generates a cylindrical wave. Due to the nature of the source and to the geometrical configuration, the transverse waves polarized in the $(\mathbf{x}_1, \mathbf{x}_2)$ plane are not excited. The present study is conducted in the plane $(O; \mathbf{x}_1, \mathbf{x}_3)$. The total elasto-acoustic wave motion will be independent of x_2, hence all derivatives with respect to x_2 vanish in the partial differential equations that govern the wave motion. Consequently coordinate x_2 is implicit in the mathematical expressions to follow.

The acoustic response is calculated in terms of pressure amplitudes at two receivers P_1 and P_2 of coordinates $(x_{1,1}, x_{1,3})$ and $(x_{2,1}, x_{2,3})$, respectively, in the plane $(O; \mathbf{x}_1, \mathbf{x}_3)$. The source, P_1 and P_2 are placed on a same line. This source and receiver configuration is typical of the device used in the ultrasonic axial transmission technique (ATT) for the evaluation of the cortical layer of bone; the angle α allows to take into account the orientation of the device with respect to the interface.

B. Equations for the fluid

The acoustic problem in the fluid is characterized by $p(\mathbf{x},t)$ and $\mathbf{v}(\mathbf{x},t)$, where $p(\mathbf{x},t)$ denotes the disturbance of the pressure from its undisturbed value at equilibrium in the reference configuration and $\mathbf{v}(\mathbf{x},t)$ is the fluid particle velocity. The components in $\mathbf{R}$ of the fluid velocity are denoted v_i.

The fluid is assumed to be homogeneous and the gravity effects are neglected in the linear acoustic equations. In the framework of the linearized theory, it is assumed that $p(\mathbf{x},t)$, $\mathbf{v}(\mathbf{x},t)$ and their gradients are small but also of the same order. The constitutive equation is defined with the inverse of the fluid compressibility denoted by K and the mass density denoted by ρ_f. The wave velocity in the fluid is then defined as $c_f = \sqrt{K/\rho_f}$ and the wave slowness as $s_f = 1/c_f$. The equation of motion and the constitutive equation are

$$\partial_i p(\mathbf{x},t) = -\rho_f \partial_t v_i(\mathbf{x},t), \quad \forall \mathbf{x} \in \Omega_1, \tag{1}$$

$$\partial_t p(\mathbf{x},t) + K\partial_i v_i(\mathbf{x},t) = K\phi_V(t)\delta(x_1, x_3 + h_s), \quad \forall \mathbf{x} \in \Omega_1. \tag{2}$$

Convention of summation on repeated indices is used. Derivatives with respect to t and x_i are denoted ∂_t and ∂_i, respectively, and $\delta(x_1, x_3)$ denotes the Dirac delta function where $x_1 = x_3 = 0$. The term on the right-hand side of Eq. (2) introduces a line source of acoustic waves parallel to $(O;\mathbf{x}_2)$ characterized by its history $\partial_t\phi_V(t)$.

C. Equations for the solid (mean solid model)

The elastodynamic problem in the solid is characterized by $\boldsymbol{\sigma}(\mathbf{x},t)$ and $\mathbf{u}(\mathbf{x},t)$, where $\boldsymbol{\sigma}(\mathbf{x},t)$ denotes the stress tensor and $\mathbf{u}(\mathbf{x},t)$ denotes the particle displacement. Their components in $\mathbf{R}$ are respectively denoted σ_{ij} and u_i.

The solid is assumed to be linear elastic, homogeneous and isotropic. The constitutive equation is defined with the Young modulus E, the Poisson ratio ν and the mass density ρ_s. The wave velocities in the solid are denoted by c_L and c_T, where the letters L and T are associated with longitudinal waves and transverse waves polarized in the direction $\mathbf{x}_3$, respectively. Waves slownesses are defined as $s_L = 1/c_L$ and $s_T = 1/c_T$.

In Section IV, E, ν and ρ_s will be modeled as random variables. In this Section, the deterministic mechanical problem is presented in terms of the mean values of the random

mechanical parameters. With the notation adopted, the mean value of a quantity is underlined: the mean values of random variables associated with E, ν and ρ_s are $\underline{E}$, $\underline{\nu}$ and $\underline{\rho}_s$, respectively. The "mean mechanical model" refers to the mechanical model for which the random parameters take their mean values.

The body force field is neglected. The equations of motion in the solid are then

$$-\partial_j \sigma_{ij}(\mathbf{x},t) + \underline{\rho}_s \partial_t^2 u_i(\mathbf{x},t) = 0, \quad \forall \mathbf{x} \in \Omega_2. \tag{3}$$

Introducing the linearized strain tensor as $\epsilon_{ij} = \frac{1}{2}(\partial_i u_j + \partial_j u_i)$ the constitutive equation (Hooke's law) is written

$$\sigma_{ij} = c_{ijkq}\epsilon_{kq}, \tag{4}$$

where c_{ijkq} is the fourth-order stiffness tensor, which is written for an isotropic solid as

$$c_{ijkq} = \frac{\underline{E}}{(1+\underline{\nu})}\left(\frac{\underline{\nu}}{(1-2\underline{\nu})}\delta_{ij}\delta_{kq} + \frac{1}{2}(\delta_{ik}\delta_{jq} + \delta_{iq}\delta_{jk})\right),$$

where δ_{ij} is the Kronecker symbol.

In the solid, the wave velocities are defined by

$$\underline{c}_L = \sqrt{\frac{\underline{E}(1-\underline{\nu})}{(1+\underline{\nu})(1-2\underline{\nu})\underline{\rho}_s}}, \quad \underline{c}_T = \sqrt{\frac{\underline{E}}{2(1+\underline{\nu})\underline{\rho}_s}}. \tag{5}$$

D. Conditions at the plane interface

At the interface $\partial\Omega$ between the fluid and the solid, the following conditions are assumed

$$v_3(\mathbf{x},t) = \partial_t u_3(\mathbf{x},t), \quad \forall \mathbf{x} \in \partial\Omega \tag{6}$$

$$\sigma_{33}(\mathbf{x},t) = -p(\mathbf{x},t), \quad \forall \mathbf{x} \in \partial\Omega \tag{7}$$

$$\sigma_{13}(\mathbf{x},t) = \sigma_{23}(\mathbf{x},t) = 0, \quad \forall \mathbf{x} \in \partial\Omega. \tag{8}$$

The continuity of the normal velocity is expressed by Eq. (6). The continuity of the pressure is depicted by Eq. (7). The condition of frictionless contact is expressed by Eq. (8).

III. SOLUTION OF THE MEAN PROBLEM

In an axial transmission ultrasonic experiment, the radio-frequency signals from the physical setup are processed following a certain procedure which yields an estimation of the velocity of longitudinal waves in the solid. This estimation is called the "apparent velocity

of longitudinal waves". In the present modeling work, a procedure that mimics the actual physical procedure is followed in which simulated signals replace the actual acoustic signals. These simulated signals are solutions of the elasto-acoustic problem defined by Eqs. (1)-(8).

This Section gives a brief account of the Cagniard-de Hoop method which is used to derive an exact semi-analytical expression of the problem defined by Eqs. (1)-(8). Next, the solution is presented. Finally, the procedure followed to calculate the apparent velocity of L-waves with simulated signals is detailed.

A. Background on the method of solution

The Cagniard-de Hoop method has been introduced by Cagniard (1939) and modified by de Hoop (1960). It is a very efficient tool for solving and investigating time-domain wave propagation problems in simple geometrical configurations. The Cagniard-de Hoop method is extensively described in the literature devoted to seismology (see Aki and Richard (1980); Kennett (1983); Pao and Gajewski (1977); van der Hijden (1987)).

With the Cagniard-de Hoop method, the solution is obtained as a sum of terms each associated with a physical wave contribution. The first step of the method consists in algebraic manipulations of the basic equations in the Fourier-Laplace domain dual of the space-time domain. In the second step, each wave contribution is identified in the Fourier-Laplace domain and transformed back to the space time domain with the Cagniard-de Hoop technique. In essence, the technique is a mathematical trick which avoids performing numerical integrations over the frequency and over the wavenumber. Finally, explicit Green's functions in the time domain for each wave contribution are derived. The response to a specific source history is calculated using convolution formulas.

The expressions derived with the Cagniard-de Hoop method are exact solutions of the wave propagation problems. Their are valid in the close field as well as in the far field.

B. Reflected wave closed form analytical solution

The fluid-solid configuration of interest in this paper has been investigated by de Hoop and van der Hijden (1983) and Grimal and Naili (2006). A detailed discussion of the method and analyses of the elasto-acoustic problem can be found in these references. The notation

used here is consistent with that used in reference Grimal and Naili (2006).

The response at a receiver in the fluid domain Ω_1 basically consists in two wave contributions: *i)* the direct wave from the source to the receiver; *ii)* the wave reflected at the interface. This reflected wave is itself the result of several wave phenomena, namely *i)* a body wave in the fluid generated from specular reflection (according to Snell-Descartes law); *ii)* lateral waves (also called "head waves"), that is, waves associated with energy propagated in the solid, close to interface, at the velocity of L- or T-waves and refracted back in the fluid; *iii)* interface waves. The direct wave path, the specular reflected wave path and the lateral wave path are sketched in Fig. 2.

The present work focuses on the lateral wave contribution because, as explained below in Section III C, it allows a direct assessment of the L-wave velocity in the solid. A theoretical presentation of lateral wave phenomena may be found in the monograph by Brekhovskikh (1960) (see p. 260); a description of the physical phenomena relative to the specific configuration investigated may be found in Bossy *et al.* (2002).

Upon application of the Cagniard-de Hoop technique to the reflected wave contribution in the Fourier-Laplace domain, the contribution of the lateral waves can be isolated from the rest of the reflected wave contributions. This is possible because lateral wave contributions are confined in a time interval $t_l < t < t_{ff}$, where t_l denotes the arrival time of the lateral wave and t_{ff} denotes the arrival time of the body wave (specular reflection). Lateral wave contributions exist only under certain conditions on the material properties of the medium. In the present work, the analysis is restricted to those cases where the lateral wave does exist and to receivers which are reached by the lateral wave. The first condition is equivalent to $\underline{c}_L > c_f$ and the second one to $\dfrac{|x_1|}{|x_3 - h_s|} > \tan\theta_c$, where θ_c is the critical angle defined by $\sin\theta_c = \dfrac{c_f}{\underline{c}_L}$ at which lateral waves are refracted and (x_1, x_3) are the coordinates of a point P in the plane $(O; \mathbf{x}_1, \mathbf{x}_3)$.

The acoustic pressure at a receiver in the fluid corresponding to the reflected waves contribution is written as

$$p_R(\mathbf{x}, t) = \partial_t \phi_V(t) * \mathcal{G}(\mathbf{x}, t), \tag{9}$$

where the operator $*$ denotes the time convolution and where $\mathcal{G}(\mathbf{x}, t)$, the Green's function for the reflected wave contribution, is given by Grimal and Naili (2006)

$$\text{if } \xi(t_{ff}) < \underline{s}_L, \quad \mathcal{G}(\mathbf{x},t) = \begin{cases} 0 & t < t_{ff} \\ \dfrac{-\rho_f}{2\pi\sqrt{t^2 - t_{ff}^2}}\, \Re[R_{ff}(\xi)] & t > t_{ff} \end{cases}$$

$$\text{if } \xi(t_{ff}) > \underline{s}_L, \quad \mathcal{G}(\mathbf{x},t) = \begin{cases} 0 & t < t_l \\ \dfrac{\rho_f}{2\pi\sqrt{t_{ff}^2 - t^2}}\, \Im[R_{ff}(\xi)] & t_l < t < t_{ff} \\ \dfrac{-\rho_f}{2\pi\sqrt{t^2 - t_{ff}^2}}\, \Re[R_{ff}(\xi)] & t > t_{ff} \end{cases} \tag{10}$$

In Eq. (10), the operators $\Re[.]$ and $\Im[.]$ are respectively the real and imaginary parts of the quantity between the brackets. In reference de Hoop and van der Hijden (1983), de Hoop and van der Hijden investigated, in the general case, the reflection at a fluid-solid interface with the Cagniard-de Hoop method. They presented a solution similar to Eq. (10), although in a slightly different form due to a difference in the formulation of the basic equations. The arrival time t_{ff} of the body wave is such that

$$t_{ff} = s_f r, \tag{11}$$

in which $r^2 = (h_s - x_3)^2 + x_1^2$ is the square of the distance between the source and the receiver. The arrival time t_l of the lateral wave contribution is defined by

$$t_l = \gamma_f(h_s - x_3) + \underline{s}_L x_1, \tag{12}$$

where $\gamma_f = \sqrt{s_f^2 - \xi^2}$. The function ξ is defined on $[0, +\infty[$ and is such that

$$\xi(\tau) = \frac{\tau x_1}{r^2} \pm i\frac{h_s - x_3}{r^2}\sqrt{\tau^2 - t_{ff}^2}. \tag{13}$$

The reflection coefficient R_{ff} at the fluid-solid interface is given by

$$R_{ff} = \frac{4\underline{\mu}\gamma_f\Delta_R - \gamma_L\rho_f\underline{s}_T^2}{4\underline{\mu}\gamma_f\Delta_R + \gamma_L\rho_f\underline{s}_T^2}, \tag{14}$$

where $\gamma_L = (\underline{s}_L^2 - \xi^2)^{1/2}$, $\gamma_T = (\underline{s}_T^2 - \xi^2)^{1/2}$, $\chi = 0.5\underline{s}_T^2 - \xi^2$ and $\Delta_R = \gamma_L\gamma_T\xi^2 + \chi^2$. The values taken by ξ must be such that $\Re[\gamma_L] \geq 0$ and $\Re[\gamma_T] \geq 0$. Lamé's coefficient $\underline{\mu}$ is defined by $\underline{\mu} = \dfrac{\underline{E}}{2(1+\underline{\nu})}$.

C. Apparent velocity of L-waves

In a typical experimental setup of the axial transmission technique, the velocity of longitudinal waves is estimated based on the lateral wave propagation. Since the estimated velocity depends on some parameters of the setup, it is referred to as the "apparent" velocity of L-waves, and denoted by v. In the ideal limit case where measurement errors are zero, the apparent velocity is equal to the longitudinal wave velocity.

The procedure for calculating v is the following:

a. Pressure signals, as shown in Fig. 3, are calculated with the Cagniard-de Hoop technique with Eq. (10) at the two receivers P_1 and P_2, separated by a distance d.

b. The arrival time of the wave is defined as the first local maximum of the pressure which corresponds to the first zero of the function $\partial_t^2 \phi_V(t) * \mathcal{G}(\mathbf{x}, t)$. The time delay separating the arrival times at the two receivers is denoted by Δt.

c. The apparent velocity of L-wave is then

$$\mathrm{v} = \frac{d}{\Delta t}. \tag{15}$$

Wave velocity v calculated by this way is in practice a good approximation of the actual velocity of longitudinal waves in the solid. The apparent velocity corresponding to the mean model is denoted $\underline{\mathrm{v}}$. Under the two following assumptions, the equality $\underline{\mathrm{v}} = \underline{c}_L$ is verified: *i)* the waveform remains unchanged during propagation between the two receivers; *ii)* the line joining the receivers is parallel to the interface ($\alpha = 0$). The first assumption is in general not verified because of close field effects (Bossy (2003); Grimal and Naili (2006)). Whether or not the second assumption is verified depends on the positioning of the ultrasonic probe with respect to the fluid-solid interface. The dependence $\underline{\mathrm{v}}(\alpha)$ is investigated in Section VII.

IV. PROBABILITY MODEL OF THE UNCERTAIN PARAMETERS

Uncertainties in the transient elasto-acoustics problem defined by Eqs. (1)-(4) with boundary conditions (6)-(8) are modeled using a parametric probabilistic approach. First,

the uncertain parameters must be identified. Then an appropriate probabilistic model must be constructed for each uncertain parameters which is modeled by a random variable.

Since the final aim of this work is the identification of the mechanical parameters of the solid, probability models are constructed for the Young modulus E, the Poisson ratio ν and the mass density ρ_s. (In a study with a different aim, one may as well consider introducing probability models for geometrical parameters and fluid parameters.)

In order to construct a coherent probability model, only the available information on the random mechanical parameters is used. This approach avoids the use of any additional speculated information that would yield a non-physical estimation of the probability distribution. In the context of information theory, Shannon (1948) introduced an entropy as the measure of uncertainty for probability distributions. In the context of statistical mechanics, Jaynes (1957a and 1957b) used this measure to define the maximum entropy principle for the construction of a probability distribution. This principle consists in maximizing the entropy subjected to constraints defined by the available information. The probability models constructed for the mechanical properties in the present work constitute particular cases of the ones described in Soize's works (Soize (2001, 2005)).

With the nature of the available information used for the probabilistic models, the application of the maximum entropy principle yields independent probability density functions for E, ν and ρ_s. In other words, the independence of the random variables associated with E, ν and ρ_s is a consequence of the use of the maximum entropy principle.

A. Young's modulus

The Young modulus is modeled by a random variable $\mathbb{E}$ with the probability density function defined using the following information: (1) The support of the probability density function is $]0, +\infty[$. (2) The mean value is such that, by construction, $\mathcal{E}\{\mathbb{E}\} = \underline{E}$, where $\mathcal{E}$ denotes the mathematical expectation. (3) The second-order moment of its inverse is finite $\mathcal{E}\{\frac{1}{\mathbb{E}^2}\} < +\infty$. Information (1) is the thermodynamic restriction on Young's modulus. Information (3) is due to the ellipticity property of the random operator modeling the elasticity tensor (see Soize (2001, 2004)). Let Y_1 be the random variable such that $\mathbb{E} = \underline{E}Y_1$, and then, $\mathcal{E}\{Y_1\} = 1$. The probability density function $f_{\mathbb{E}}$ of $\mathbb{E}$ is such that $f_{\mathbb{E}}(E)dE = f_{Y_1}(y_1)dy_1$. To construct the probability density function, information (3) is taken into

account by requiring that $\mathcal{E}\{\ln(Y_1)\} = c_1$ with $c_1 < +\infty$, where ln designates the natural logarithm function (see Soize (2001)). To summarize, the probability density function f_{Y_1} whose support is $]0, +\infty[$ has to verify the following constraints

$$\begin{cases} \displaystyle\int_{-\infty}^{+\infty} f_{Y_1}(y_1)dy_1 = 1, \quad \int_{-\infty}^{+\infty} y_1 \; f_{Y_1}(y_1)dy_1 = 1, \\ c_1 < +\infty \quad \text{with} \quad c_1 = \displaystyle\int_{-\infty}^{+\infty} \ln(y_1) \; f_{Y_1}(y_1)dy_1. \end{cases} \tag{16}$$

The application of the maximum entropy principle yields the probability density function of Y_1

$$f_{Y_1}(y_1) = \mathbb{1}_{]0,+\infty[}(y_1) \exp(-\lambda_0 - \lambda_1 y_1) \; y_1^{-\lambda_2}, \tag{17}$$

where $\mathbb{1}_{]0,+\infty[}(y)$ is such that for $B \subset \mathbb{R}$, $\mathbb{1}_B(y) = 1$ if $y \in B$ and 0 if $y \notin B$, where $\mathbb{R}$ designates the set of real numbers. The three Lagrange multipliers λ_0, λ_1 and λ_2 introduced in Eq. (17) are real numbers associated with the three constraints defined by Eq. (16) and can be obtained in close form: $\lambda_0 = -\ln(\frac{\lambda_1^{\lambda_1}}{\Gamma(\lambda_1)})$, $\lambda_1 = \frac{1}{\delta_1^2}$ and $\lambda_2 = 1 - \lambda_1$, where $\delta_1^2 = \mathcal{E}\{Y_1^2\} - 1$ is the variance of Y_1. Parameter δ_1 is the coefficient of variation of the random variable Y_1 and can be used to control the dispersion of Y_1 and, consequently, of the random variable $\mathbb{E}$. Using the obtained expressions, Eq. (17) yields

$$f_{Y_1}(y_1) = \mathbb{1}_{]0,+\infty[}(y_1) \; (\tfrac{1}{\delta_1^2})^{\frac{1}{\delta_1^2}} \; \tfrac{1}{\Gamma(\delta_1^{-2})} \; y_1^{\frac{1}{\delta_1^2}-1} \; \exp(-\tfrac{y_1}{\delta_1^2}), \quad \text{with } 0 \leq \delta_1 \leq 1/\sqrt{2} \tag{18}$$

where $\Gamma(x) = \displaystyle\int_0^{+\infty} t^{x+1}x^t dt$ is the Gamma function.

B. Poisson's ratio

The Poisson ratio is modeled by a random variable Y_2 with the probability density function defined using the following information: (1) The support of the probability density function is $]-1, 1/2[$. (2) By construction, $\mathcal{E}\{Y_2\} = \underline{\nu}$. (3) $\mathcal{E}\{\dfrac{(1-Y_2)^2}{(1+Y_2)^2(1-2Y_2)^2}\} = c_2$, with $c_2 < +\infty$. Information (1) is the thermodynamic restriction on Poisson's ratio. Information (3) is a non trivial condition which is required to ensure that the second-order moments of the wave velocities are finite. The derivation of this condition is detailed in Appendix A.

To summarize, the probability density function f_{Y_2} whose support is $]-1, 1/2[$ has to

verify the following constraints

$$\begin{cases} \displaystyle\int_{-\infty}^{+\infty} f_{Y_2}(y_2)dy_2 = 1, & \displaystyle\int_{-\infty}^{+\infty} y_2\ f_{Y_2}(y_2)dy_2 = \underline{\nu}, \\ c_2 < +\infty \quad \text{with} \quad c_2 = \displaystyle\int_{-\infty}^{+\infty} \frac{(1-y_2)^2}{(1+y_2)^2(1-2y_2)^2} f_{Y_2}(y_2)dy_2. \end{cases} \tag{19}$$

The application of the maximum entropy principle yields the probability density function of Y_2

$$f_{Y_2}(y_2) = \mathbb{1}_{]-1,1/2[}(y_2)\ \exp(-\lambda_0 - \lambda_1 y_2 - \lambda_2 \frac{(1-y_2)^2}{(1+y_2)^2(1-2y_2)^2}), \tag{20}$$

where the Lagrange multipliers λ_0, λ_1 and λ_2 can not be found in closed form. They are obtained by minimizing the strictly convex function $H_2(\lambda_0, \lambda_1, \lambda_2)$ defined by

$$H_2(\lambda_0, \lambda_1, \lambda_2) = \lambda_0 + \lambda_1 \underline{\nu} + \lambda_2 c_2 + \int_{-1}^{1/2} \exp(-\lambda_0 - \lambda_1 y_2 - \lambda_2 \frac{(1-y_2)^2}{(1+y_2)^2(1-2y_2)^2}) dy_2. \tag{21}$$

The strictly convex optimization problem is solved by an usual numerical method (Ciarlet (1989)) and c_2 is rewritten as a function of the coefficient of variation $\delta_2 = \sigma_{Y_2}/\underline{\nu}$ of random variable Y_2, where σ_{Y_2} is the standard deviation given by Eq. (20). Parameter δ_2 allows the dispersion to be controlled. Fig. 4 displays the probability density function f_{Y_2} for $\delta_2 = 0.05$ (dash-dotted line), 0.1 (solid line) and 0.2 (dashed line).

C. Mass density

The mass density is modeled by a random variable R for which the available information is the following: (1) The support of the probability density function is $]0, +\infty[$. (2) By construction, $\mathcal{E}\{\mathrm{R}\} = \underline{\rho}_s$. (3) $\mathcal{E}\{\frac{1}{\mathrm{R}^2}\} < +\infty$. Information (1) is the thermodynamic restriction on mass density. Information (3) is required to get a second-order solution of the stochastic problem (see Soize (2001, 2004)). Let Y_3 be the random variable such that $\mathrm{R} = \underline{\rho}_s Y_3$, and then, $\mathcal{E}\{Y_3\} = 1$. The probability density function f_{R} of R is such that $f_{\mathrm{R}}(\rho_s)d\rho_s = f_{Y_3}(y_3)dy_3$. Information (3) is taken into account by requiring that $\mathcal{E}\{\ln(Y_3)\} = c_3$ with $c_3 < +\infty$. To summarize, the probability density function f_{Y_3} whose support is $]0, +\infty[$ has to verify the following constraints

$$\begin{cases} \displaystyle\int_{-\infty}^{+\infty} f_{Y_3}(y_3)dy_3 = 1, & \displaystyle\int_{-\infty}^{+\infty} y_3\ f_{Y_3}(y_3)dy_3 = 1, \\ c_3 < +\infty \quad \text{with} \quad c_3 = \displaystyle\int_{-\infty}^{+\infty} \ln(y_3)\ f_{Y_3}(y_3)dy_3. \end{cases} \tag{22}$$

These constraints are the same as those verified by the probability density function f_{Y_1}. Using the same method as in Section IV A yields

$$f_{Y_3}(y_3) = \mathbb{1}_{]0,+\infty[}(y_3)\ (\tfrac{1}{\delta_3^2})^{\frac{1}{\delta_3^2}}\ \tfrac{1}{\Gamma(\delta_3^{-2})} y_3^{\frac{1}{\delta_3^2}-1}\ \exp(-\tfrac{y_3}{\delta_3^2}),\quad \text{with } 0 \leq \delta_3 \leq 1/\sqrt{2} \tag{23}$$

where $\delta_3^2 = \mathcal{E}\{Y_3^2\} - 1$ is the variance of Y_3. The coefficient of variation δ_3 can be used to control the dispersion of the random variable Y_3 and, consequently, on the random variable R.

V. STOCHASTIC SOLVER FOR THE UNCERTAIN MECHANICAL SYSTEM

The stochastic solver used is based on a Monte Carlo numerical simulation. First, realizations of random variable $\mathbf{Y} = (Y_1, Y_2, Y_3)$ are constructed. For each realization of $\mathbf{Y}$, the corresponding realization of the random apparent velocity V is calculated. Finally, the mathematical statistics are used for constructing the estimations and a convergence analysis is performed with respect to the number of realizations.

A. Acoustic pressure

The first step consists in constructing, with the adapted generator, independent realizations $\mathbf{Y}(\theta_1), \ldots, \mathbf{Y}(\theta_n)$ using the probability density functions defined by Eqs. (18), (20) and (23). In a second step, the quantities $\mathrm{V}(\theta_1), \ldots, \mathrm{V}(\theta_n)$ are calculated using the procedure described in Section III with the solution Eqs. (9)-(14) obtained with the Cagniard-de Hoop method, and Eq. (15). The equations of Section III B are rewritten below in order to exhibit the random quantities.

For each realization θ_j $(j = 1, ..., n)$, the pressure at the receiver is given by

$$P_R(\mathbf{x}, t, \theta_j) = \partial_t \phi_V(t) * \mathrm{G}(\mathbf{x}, t, \theta_j), \tag{24}$$

where G is the Green function given by

$$\text{if } \xi(t_{ff}) < S_L(\theta_j), \quad \mathrm{G}(\mathbf{x},t,\theta_j) = \begin{cases} 0 & t < t_{ff} \\ \dfrac{-\rho_f}{2\pi\sqrt{t^2 - t_{ff}^2}}\, \Re[R_{ff}(\xi,\theta_j)] & t > t_{ff} \end{cases}$$

$$\text{if } \xi(t_{ff}) > S_L(\theta_j), \quad \mathrm{G}(\mathbf{x},t,\theta_j) = \begin{cases} 0 & t < T_l(\theta_j) \\ \dfrac{\rho_f}{2\pi\sqrt{t_{ff}^2 - t^2}}\, \Im[R_{ff}(\xi,\theta_j)] & T_l(\theta_j) < t < t_{ff} \\ \dfrac{-\rho_f}{2\pi\sqrt{t^2 - t_{ff}^2}}\, \Re[R_{ff}(\xi,\theta_j)] & t > t_{ff} \end{cases}, \tag{25}$$

where $S_L = 1/C_L$ and $S_T = 1/C_T$ are the random variables modeling the waves slownesses respectively associated with s_L and s_T. The arrival time of the body wave t_{ff} is defined by Eq. (11). In contrast, in the probabilistic model, the arrival time of the lateral wave contribution is modeled by the random variable T_l defined by

$$T_l = \gamma_f(h_s - x_3) + S_L x_1. \tag{26}$$

The function ξ is given by Eq. (13). The realization $R_{ff}(\xi,\theta_j)$ of the random reflection coefficient associated with $R_{ff}(\xi)$ is written as

$$R_{ff}(\xi,\theta_j) = \frac{4\mu_j\gamma_f\Delta_{R,j} - \gamma_{L,j}\rho_f S_{T,j}^2}{4\mu_j\gamma_f\Delta_{R,j} + \gamma_{L,j}\rho_f S_{T,j}^2}, \tag{27}$$

where $\gamma_{L,j} = \left(S_L^2(\theta_j) - \xi^2\right)^{1/2}$, $\gamma_{T,j} = \left(S_T^2(\theta_j) - \xi^2\right)^{1/2}$, $\chi_j = 0.5S_T^2(\theta_j) - \xi^2$ and $\Delta_{R,j} = \gamma_{L,j}\gamma_{T,j}\xi^2 + \chi_j^2$. Realization jth of the random variable associated with μ is defined by $\mu_j = \dfrac{\underline{E}Y_1(\theta_j)}{2(1 + Y_2(\theta_j))}$.

B. Convergence analysis

The convergence analysis with respect to n is carried out in studying the convergence of the estimated second-order moment of V, defined by $m_{\mathrm{V},2} = \mathcal{E}\{\mathrm{V}^2\}$. An estimation of $m_{\mathrm{V},2}$ is provided by $m_{\mathrm{V},2} \simeq \mathrm{Conv}^2(n)$ where

$$\mathrm{Conv}^2(n) = \frac{1}{n}\sum_{j=1}^{n} \mathrm{V}(\theta_j)^2. \tag{28}$$

The graphs of functions $n \to \log_{10}\left(\mathrm{Conv}^2(n)\right)$ for different values of the coefficients of variation $(\delta_1, \delta_2, \delta_3)$ are shown in Fig. 5, where $\log_{10}$ is the base 10 logarithm function. The

dash-dotted line represents the case for which $\delta_1 = \delta_2 = \delta_3 = 0.05$. The solid line, the case for which $\delta_1 = \delta_2 = \delta_3 = 0.1$. And the dashed line, the case for which $\delta_1 = \delta_2 = \delta_3 = 0.2$. Convergence is reached for $n > 1\ 000$, $n > 2\ 000$, and $n > 3\ 500$ in the three cases, respectively.

C. Estimation of the mean value and of the confidence region

Let $\mathrm{v}_1 = \mathrm{V}(\theta_1), \ldots, \mathrm{v}_n = \mathrm{V}(\theta_n)$ be the n calculated independent realizations of the random variable V. Estimations of mathematical expectation $\mathcal{E}\{\mathrm{V}\}$ and coefficient of variation δ_V are given by

$$\mathcal{E}\{\mathrm{V}\} \simeq \hat{\underline{\mathrm{V}}} = \frac{1}{n}\sum_{j=1}^{n} \mathrm{v}_j \quad \text{and} \quad \delta_\mathrm{V} \simeq \frac{n}{\sqrt{n-1}} \frac{\sqrt{\sum_{j=1}^{n} (\mathrm{v}_j - \frac{1}{n}\sum_{k=1}^{n} \mathrm{v}_k)^2}}{\sum_{j=1}^{n} \mathrm{v}_j} \quad . \tag{29}$$

The quantile method is used to construct the confidence region associated with a probability level P_c for random variable V. The confidence region is limited by a lower and an upper envelope denoted v^- and v^+, respectively

$$\mathcal{P}(\mathrm{v}^- < \mathrm{V} \leq \mathrm{v}^+) = P_c. \tag{30}$$

Let F_V be the cumulative distribution function (continuous from the right) of V defined by $F_\mathrm{V}(\mathrm{v}) = \mathcal{P}(\mathrm{V} \leq \mathrm{v})$. For $0 < p < 1$, the pth quantile (or fractile) of F_V is defined as

$$\zeta(p) = \inf\{\mathrm{v} : F_\mathrm{V}(\mathrm{v}) \geq p\}. \tag{31}$$

The lower and the upper envelopes for the symmetric interval are defined by

$$\mathrm{v}^- = \zeta(\frac{1-P_c}{2}), \quad \mathrm{v}^+ = \zeta(\frac{1+P_c}{2}). \tag{32}$$

The estimations of v^- and v^+ are performed by using the sample quantiles (Serfling (1980)). Let $\tilde{\mathrm{v}}_1 < \ldots < \tilde{\mathrm{v}}_n$ be the order statistics associated with $\mathrm{v}_1, \ldots, \mathrm{v}_n$. Therefore, we have the following estimations

$$\mathrm{v}^- \simeq \tilde{\mathrm{v}}_{j^-} \quad \text{with} \quad j^- = \mathrm{fix}(n(1-P_c)/2), \tag{33}$$

$$\mathrm{v}^+ \simeq \tilde{\mathrm{v}}_{j^+} \quad \text{with} \quad j^+ = \mathrm{fix}(n(1+P_c)/2), \tag{34}$$

in which $\mathrm{fix}(z)$ is the integer part of real number z.

VI. CALCULATION PARAMETERS AND VALIDATION OF THE MEAN MODEL

This Section presents the parameters used for the calculation (source history and numerical data used for the mean model) and some calculations used for the validation of the mean model.

A. A set of cortical bone samples

Dong and Guo (2004) performed mechanical tests and measured the porosity of a set of eighteen cortical bone samples obtained from six human femurs. The authors introduced the usual assumption that cortical bone can be viewed as a homogeneous, linear elastic and transversely isotropic material with the plane of isotropy perpendicular to the long axis of the bone. Accordingly, five elastic parameters were measured. Eighteen values were obtained for each measured parameter. Then Dong and Guo (2004) performed mathematical statistics to calculate the mean value and the standard deviation of each parameter.

In the present work, bone is modeled as an isotropic solid. Since the work focuses on the measurement of the longitudinal wave velocity along the axis of bone, only $E = E_1$, where E_1 is the Young modulus corresponding to solicitation of the bone along this axis is used in the present work. Based on their experimental values, Dong and Guo (2004) give a mean value of $\underline{E_1} = 16.61 \times 10^9$ Pa and a value of the standard deviation, for the set of eighteen samples, of $\pm 1.83 \times 10^9$ Pa.

The mean value of the porosity ϕ for the set of samples is $\underline{\phi} = 8.95\%$ with a standard deviation of $\pm 4.16\%$. For the purposes of the present work, the density has been calculated based on the given values of porosity by using the formula

$$\rho_s = \rho_t(1 - \phi), \tag{35}$$

where ρ_t is the mass density of the bone tissue (around the pores). The bone tissue mass density has been calculated from the data published by Raum *et al.* (2006), $\rho_t = 1\ 891$ kg.m^{-3}. In the present work, ρ_t is considered to be a "universal" value valid for every bone sample; as a consequence, ρ_t is modeled as deterministic. The mean value of the mass density is then $\underline{\rho_s} = (1 - \underline{\phi})\rho_t = 1\ 722$ kg.m^{-3} and the standard deviation for the set of eighteen samples is ± 78.7 kg.m^{-3}.

B. Acoustic source

The history of the acoustic source is defined by the function

$$\partial_t \phi_V(t) = \sin(2\pi t f) \exp(-4(tf-1)^2) \tag{36}$$

where f is the center frequency of the pulse. In this paper, calculations are performed with $f = 1$ Mhz. Figure 6 displays the graph of the function $t \to \partial_t \phi_V(t)$.

C. Data for the mean model

The source is located at $h_s = 2$ mm from the interface. The distance between the source and the first receiver is 20 mm. The distance between the receivers is 2 mm. The fluid is supposed to be water: $\rho_f = 1\ 000$ kg.m^{-3} and $c_f = 1\ 490$ m.s^{-1}.

The mean values of the solid (bone) parameters are adapted from the experimental results detailed in section VI A. Only the mean values of E and ρ obtained from the data of Dong and Guo (2004) have been used as input in the probability density functions of the random variables. In particular, the standard deviations derived from the experimental measurements were not used. Indeed, the standard deviation is not taken to be an available information for the construction of the probabilistic models with the maximum entropy principle. This is consistent with the fact that the number of bone samples measured in the experiments of Dong and Guo is too small to provide converged second-order moments (standard deviations) of the measured parameters.

The mean model is defined with $\underline{E} = 16.61 \times 10^9$ Pa and $\underline{\rho}_s = 1\ 722$ kg.m^{-3}. The mean value of the isotropic Poisson's ratio is taken to be $\underline{\nu} = 0.3$, which is the value usually assumed in bone (Zysset *et al.* (1999)). With these values for the mean model, $\underline{c}_L = 3\ 604$ m.s^{-1}.

D. Validation

A first validation of the mean model has been obtained by comparing the calculated velocities with velocity measurements on several materials reported in Bossy's thesis (Bossy (2003)) (see p. 69-71), in an axial transmission experiment setup, for different distances between the source and the receivers. A second validation of the mean model was obtained by comparing the calculated velocities for several values of the angle α with velocities calculated

by Bossy (Bossy (2003)) (see p. 107-110), in the same geometrical configuration, with the help of a finite differences code based on Virieux's numerical scheme (Virieux (1986)).

VII. RESULTS

A. Mean value and dispersion of the apparent velocity

This section focuses on the case $\alpha = 0$. The sensitivity of the apparent velocity v to each of the mechanical parameters (E, ν and ρ_s) is presented. Each of the coefficients of variation δ_i ($i = 1, 2, 3$), associated with E, ν and ρ_s, respectively, varies separately. For this purpose, three cases are defined: Case 1 ($\delta_1 = \delta$, $\delta_2 = \delta_3 = 0$); Case 2 ($\delta_2 = \delta$, $\delta_1 = \delta_3 = 0$); and Case 3 ($\delta_3 = \delta$, $\delta_1 = \delta_2 = 0$), where δ takes the values $0.05, 0.1$, and 0.2, successively.

With the values defined for the mean model, $\underline{\mathrm{v}} = 3\ 574$ m.s^{-1}. The difference between $\underline{c}_L = 3\ 604$ m.s^{-1} and $\underline{\mathrm{v}}$ is due to the changes in the shape of the response between the two receivers.

The estimated mean values $\underline{\hat{\mathrm{V}}}$ for Cases 1-3 are collected in Table I. Note that: *i)* $\underline{\hat{\mathrm{V}}} < \underline{\mathrm{v}}$ in Case 1, while $\underline{\hat{\mathrm{V}}} > \underline{\mathrm{v}}$ in Cases 1 and 2; *ii)* the values of $\underline{\hat{\mathrm{V}}}$ decrease with dispersion in Case 1 while they increase Cases 1 and 2; *iii)* the value of $\underline{\hat{\mathrm{V}}}$ is more sensitive to the dispersion on $\nu(\delta_2)$ and $\rho_s(\delta_3)$ than on the dispersion on $E(\delta_1)$.

The confidence regions of the calculated apparent wave velocity for $P_c = 0.95$ are plotted in Fig. 7-9 for Cases 1-3. The width of the confidence regions are $345, 684$, and $1\ 348$ m.s^{-1} in Case 1 for the three dispersion levels, respectively; $288, 566$, and $1\ 160$ m.s^{-1} in Case 2; $347, 716$, and $1\ 416$ m.s^{-1} in Case 3. The width of the confidence regions are of the same order of magnitude, however the values indicate that the apparent velocity is slightly more sensitive to variations of E and ρ_s than to variations of ν. One may also note that the upper and lower envelopes are not symmetric with respect to mean values.

B. Sensitivity analysis with respect to angle α

The evolution of the distribution of V with respect to α and the dispersion levels on the random mechanical parameters are shown in Fig. 10. Angle α varies in $[-5, 5]$ (values given in degrees (deg)) with a sampling angle step 0.5 deg. The upper and lower envelopes of the confidence region ($P_c = 0.95$) of V *versus* α are represented by dash-dotted lines in case

$\delta_1 = \delta_2 = \delta_3 = 0.05$, by solid lines in case $\delta_1 = \delta_2 = \delta_3 = 0.1$, and by dashed lines in case $\delta_1 = \delta_2 = \delta_3 = 0.2$. The thin solid line represents the apparent velocity $\underline{v}$ obtained from the mean model. In Fig. 10, $\underline{v}$ was plotted in order to allow the comparison between the random modeling of the axial transmission experiment and a deterministic modeling (model with the values of the mean model). Both $\underline{v}$ and the widths of the confidence regions are decreasing functions of α. In essence, this is due to the evolution with α of the wave paths of the waves arriving at the two receivers. In addition, the upper and the lower envelopes are not symmetric with respect to $\underline{v}$. The ratio of the width of the confidence region for a given set of coefficients of variation and $\underline{v}$ depends weakly on α. In other words, the orientation of the receivers line has a weak influence on the normalized confidence region.

VIII. CONCLUSION

As far as we know, this paper presents the first probabilistic model of the ultrasonic axial transmission technique. This technique can measure the longitudinal wave velocity of an immersed solid, based on the propagation of a lateral wave. This work did not focus on the velocity of longitudinal waves itself but rather on an apparent velocity of longitudinal waves, as measured by existing devices. This was done in order to include some measurement constraints in the model. Measurement constraints were modeled as deterministic parameters while the material parameters of the sounded solid were modeled as random parameters. The reason for this choice is that we are interested in measuring solids with random mechanical parameters while the measurement errors are supposed to be well controlled.

The developed random model of the axial transmission technique was used to predict the apparent velocity when the solid is cortical bone. The probability density functions constructed for the random Young's modulus and the random mass density are such that their mean values are equal to mean value calculated for a set of eighteen bone samples with mathematical statistics. The values of the coefficients of variation δ_i used in the simulations for the random mechanical parameters are of the same order of magnitude as the physiological dispersion levels for cortical bone. However, the validity of the many assumptions must be tested in future work, in particular the assumptions concerning bone isotropy.

The analysis has revealed a complex behavior of the apparent velocity with respect to the levels of dispersion of the bone material parameters. In particular, *i)* the estimated mean

value of the apparent velocity varies with the coefficients of variation, and its behavior is different with respect to these coefficients on each mechanical parameter; *ii)* the apparent velocity is more sensitive to variations of Young's modulus or mass density than to variations of Poisson's ratio; *iii)* the angle α between the fluid-solid interface and the source-receiver line has a strong influence on the mean value and on the width of the confidence region.

Appendix A: CONDITIONS ON THE WAVE VELOCITIES

Because the aim of this work is to model a technique which allows an estimation of the longitudinal wave velocity to be constructed, particular attention is paid to the moments of the velocities. At least, the second-order moment of C_L and C_T must be finite.

a. Longitudinal wave velocity. The condition is written

$$\exists\, q \in \mathbb{N}^* \quad \text{such that} \quad \mathcal{E}\{C_L^{2q}\} < +\infty. \tag{A1}$$

where $\mathbb{N}^*$ is the set of non-zero integers.

Using the expression of C_L deduced from Eq. (5) yields

$$\exists\, q \in \mathbb{N}^* \quad \text{such that} \quad \mathcal{E}\{C_L^{2q}\} = \mathcal{E}\{\frac{\mathbb{E}^q(1-Y_2)^q}{(1+Y_2)^q(1-2Y_2)^q \mathrm{R}^q}\}. \tag{A2}$$

Since random variables $\mathbb{E}, Y_2$ and R are mutually independent, then

$$\mathcal{E}\{C_L^{2q}\} = \mathcal{E}\{\mathbb{E}^q\}\mathcal{E}\{\frac{1}{\mathrm{R}^q}\}\mathcal{E}\{\frac{(1-Y_2)^q}{(1+Y_2)^q(1-2Y_2)^q}\}. \tag{A3}$$

By construction, random variable $\mathbb{E}$ has a finite second-order moment (Section IV A). In Section IV B, the third information on the Poisson ratio is $\mathcal{E}\{\frac{(1-Y_2)^2}{(1+Y_2)^2(1-2Y_2)^2}\} < +\infty$. Finally, in Section IV C, the third information on the mass density is $\mathcal{E}\{\frac{1}{\mathrm{R}^2}\} < +\infty$. Then Eq. (A1) holds for $q = 2$. The finite fourth-order moment of longitudinal wave velocity C_L implies a finite second-order moment of C_L.

b. Transverse wave velocity. In order to use the third information on Y_2, we write

$$\frac{(1-Y_2)^2}{(1+Y_2)^2(1-2Y_2)^2} = \left(\frac{2}{3(1+Y_2)} + \frac{1}{3(1-2Y_2)}\right)^2. \tag{A4}$$

The mathematical expectation of the left-hand of Eq. (A4) is finite (see Section IV B). Taking the mathematical expectation of Eq. (A4) yields

$$\mathcal{E}\{\frac{(1-Y_2)^2}{(1+Y_2)^2(1-2Y_2)^2}\} = \mathcal{E}\{\frac{4}{9(1+Y_2)^2}\} + \mathcal{E}\{\frac{4}{9(1+Y_2)(1-2Y_2)}\} + \mathcal{E}\{\frac{1}{9(1-2Y_2)^2}\}. \quad \text{(A5)}$$

Because each terms on the right-hand of Eq. (A5) is strictly positive and finite

$$\mathcal{E}\{\frac{1}{(1+Y_2)^2}\} < +\infty. \quad \text{(A6)}$$

Since the random variable C_T modeling the transverse wave velocity is such that

$$C_T^4 = \frac{\mathbb{E}^2}{4(1+Y_2)^2\mathrm{R}^2}, \quad \text{(A7)}$$

then, the fourth-order moment of C_T is finite and consequently, its second-order moment is finite.

References

Aki, K. and Richard, P. (**1980**), *Quantitative seismology: theory and methods* (Freeman, San Francisco).

Bossy, E. (**2003**), "Évaluation ultrasonore de l'os cortical par transmission axiale : modélisation et expérimentation *in vitro* et *in vivo*," PhD thesis, Université Pierre et Marie Curie.

Bossy, E., Talmant, M., Defontaine, M., Patat, F., and Laugier, P. (**2004**), "Bidirectional axial transmission can improve accuracy and precision of ultrasonic velocity measurement in cortical bone: a validation on test materials," IEEE Transactions on Ultrasonics, Ferroelectrics and Frequency Control **51**(1), 71–79.

Bossy, E., Talmant, M., and Laugier, P. (**2002**), "Effect of bone cortical thickness on velocity measurement using ultrasonic axial transmission: a 2D simulation study," Journal of Acoustical Society of America **112**, 297–307.

Brekhovskikh, L. (**1960**), *Waves in layered media* (Academic Press).

Cagniard, L. (**1939**), *Réflexion et réfraction des ondes séismiques progressives. [Translated and revised by E.A. Flinn et C.H. Dix, Reflection and refraction of progressive seismic waves. Mc-Graw Hill, New York, 1962.]* (Gauthier-Villars, Paris).

Ciarlet, P. (**1989**), *Introduction to numerical linear algebra and optimisation* (Cambridge University Press, Cambridge).

de Hoop, A. (**1960**), "A modification of Cagniard's method for solving seismic pulse problems," Applied Scientific Research **8**, 349–356.

de Hoop, A. and van der Hijden, J. (**1983**), "Generation of acoustic waves by an impulsive line source in a fluid/solid configuration with a plane boundary," Journal of the Acoustical Society of America **74**(4), 333–342.

Dong, X. and Guo, X. (**2004**), "The dependence of transversaly isotropic elasticity of human femoral cortical bone on porosity," Journal of Biomechanics **37**, 1281–1287.

Foldes, A., Rimon, A., Keinan, D., and Popovtzer, M. (**1995**), "Quantitative ultrasound of the tibia: A novel approach for assessment of bone status," Bone **17**, 363–367.

Grimal, Q. and Naili, S. (**2006**), "A theoretical analysis in the time-domain of wave reflection on a bone plate," Journal of Sound and Vibration , Forthcoming.

Jaynes, E. (**1957**a), "Information theory and statistical mechanics," The Physical Review **106**(4), 620–630.

Jaynes, E. (**1957**b), "Information theory and statistical mechanics. II," The Physical Review **108**(2), 171–190.

Kapur, J. and Kesavan, H. (**1992**), *Entropy optimization principles with applications* (Academic Press, New York).

Kennett, B. (**1983**), *Seismic wave propagation in stratified media* (Cambridge University Press).

Lowet, G. and Van der Perre, G. (**1996**), "Ultrasound velocity measurements in long bones: measurement method and simulation of ultrasound wave propagation," Journal of Biomechanics **29**, 1255–1262.

Pao, Y. and Gajewski, R. (**1977**), "The generalized ray theory and transient response of layered elastic solids," in *Physical Acoustics*, edited by W. Mason and R. Thurston (Academic Press, New York), vol. XIII, pp. 183–265.

Raum, K., Cleveland, R., Peyrin, F., and Laugier, P. (**2006**), "Derivation of elastic stiffness from site-matched mineral density and acoustic impedance maps," Phys. Medicine and Biology **Forthcoming**.

Serfling, R. (**1980**), *Approximation theorems of mathematical statistics* (Wiley, New York).

Shannon, C. (**1948**), "A mathematical theory of communication," Bell System Technology Journal **27**, 379–423.

Soize, C. (**2001**), "Maximum entropy approach for modeling random uncertainties in tran-

sient elastodynamics," Journal of Acoustical Society of America **109**(5), 1979–1996.

Soize, C. (**2004**), "Random-field model for the elasticity tensor of anisotropic random media," Comptes Rendus Mecanique **332**, 1007–1012.

Soize, C. (**2005**), "Random matrix theory for modeling uncertainties in computational mechanics," Computer Methods in Applied Mechanics and Engineering **194**, 1333–1366.

van der Hijden, J. (**1987**), *Propagation of transient elastic waves in stratified anisotropic media*, vol. 32 of *Applied Mathematics and Mechanics* (North Holland, Elsevier Science Publishers, Amsterdam).

Virieux, J. (**1986**), "*P-SV* Wave propagation in heterogeneous media: velocity-stress finite-difference method," Geophysics **51**(4), 889–901.

Zysset, P., Guo, X., Hoffler, C., Moore, K., and Goldstein, S. (**1999**), "Elastic modulus and hardness of cortical and trabecular bone lamellae measured by nanoindentation in the human femur," Journal of Biomechanics **32**(10), 1005–1012.

Table I. Estimation of mathematical expectation $\mathcal{E}\{\mathrm{V}\}$, standard deviation σ_{V} and coefficient of variation δ_{V} of the apparent wave velocity V.

$\underline{\mathrm{v}}$ (m.s^{-1})	3 574	3 574	3 574	3 574	3 574	3 574	3 574	3 574	3 574
δ_1	0.05	0.1	0.2	0.	0.	0.	0.	0.	0.
δ_2	0.	0.	0.	0.05	0.1	0.2	0.	0.	0.
δ_3	0.	0.	0.	0.	0.	0.	0.05	0.1	0.2
$\mathcal{E}\{\mathrm{V}\} \simeq \underline{\hat{\mathrm{V}}}$ (m.s^{-1})	3 573	3 570	3 551	3 580	3 600	3 670	3 578	3 586	3 632
σ_{V} (m.s^{-1})	89	179	347	73	147	301	90	181	363
$\delta_{\mathrm{V}}(10^{-2})$	2.49	5.01	9.77	2.04	4.08	8.21	2.51	5.05	9.99

LIST OF FIGURES

1 Model configuration. Receivers are located at points P_1 and P_2. 28

2 Wave paths. The three types of wave paths are sketched: direct waves, reflected waves and lateral waves (bold line). 29

3 Acoustic response $p_R(\mathbf{x}, t)$ *versus* times at $P_1(20, -2)$ (solid line) $P_2(22, -2)$ (dashed line), dimensions in mm. Evaluated time of flights are denoted by crosses. 30

4 Probability density function of random variable Y_2 modeling the Poisson ratio for coefficient of variation $\delta_2 = 0.05$ (dash-dotted line), $\delta_2 = 0.1$ (solid line) and $\delta_2 = 0.2$ (dashed line). 31

5 Convergence of the estimated second-order moment of V with respect to n. The coefficients of variation δ_i $(i = 1, 2, 3)$ are all set to the same value: $\delta_i = 0.05$ (thin line), $\delta_i = 0.1$ (medium line); $\delta_i = 0.2$ (thick line). 32

6 History of acoustic source $\partial_t \phi_V(t)$ with 1 MHz center frequency. 33

7 Confidence region for a probability level of $P_c = 0.95$ (dashed line) and estimated mean value (solid line) of the random variable V *versus* the coefficient of variation associated to the Young's modulus. 34

8 Confidence region for a probability level of $P_c = 0.95$ (dashed line) and estimated mean value (solid line) of the random variable V *versus* the coefficient of variation associated to the Poisson ratio. 35

9 Confidence region for a probability level of $P_c = 0.95$ (dashed line) and estimated mean value (solid line) of the random variable V *versus* the coefficient of variation associated to the mass density. 36

10 Confidence region of random variable V *versus* angle α for a fixed level of probability $P_c = 0.95$. Each plot (*i.e.* two similar lines) is associated to a single value of the coefficients of variation of the uncertain parameters δ_i $(i = 1, 2, 3)$; $\delta_i = 0.05$ (dash-dotted line), $\delta_i = 0.1$ (solid line) $\delta_i = 0.2$ (dashed line). The apparent velocity of longitudinal waves $\underline{\mathrm{v}}$ obtained for the mean model *versus* angle α is plotted in solid thin line. 37

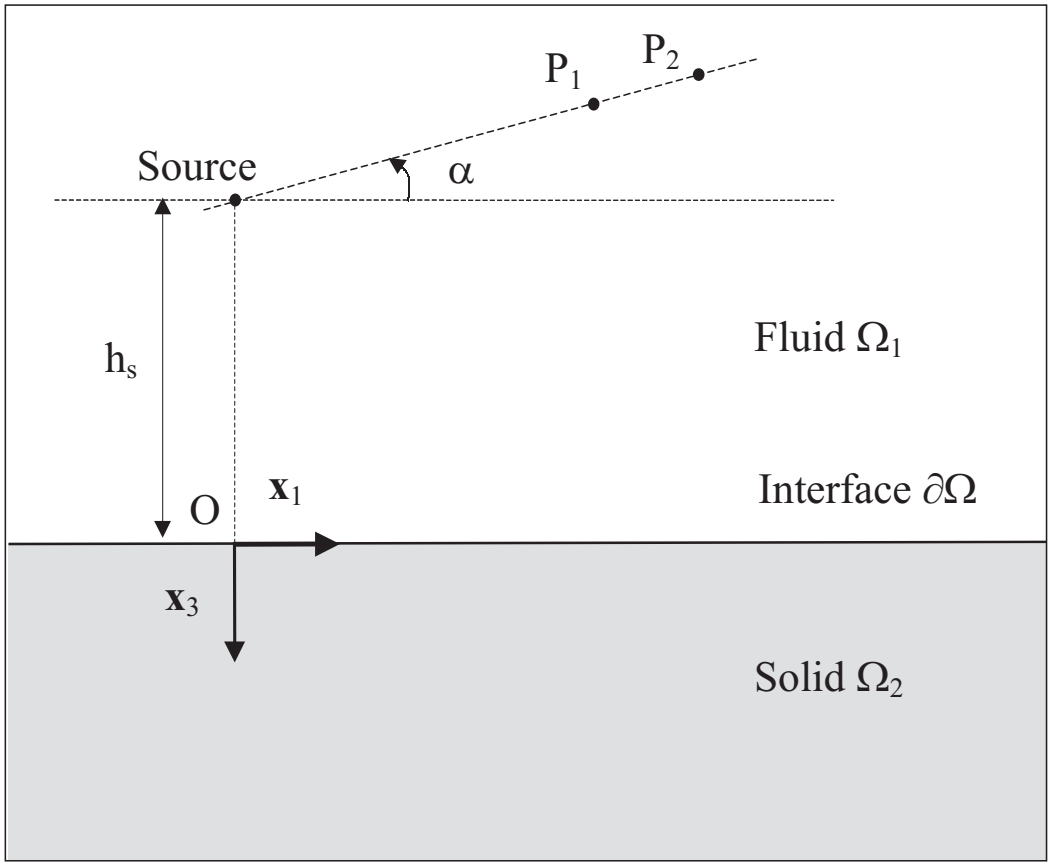

Figure 1.

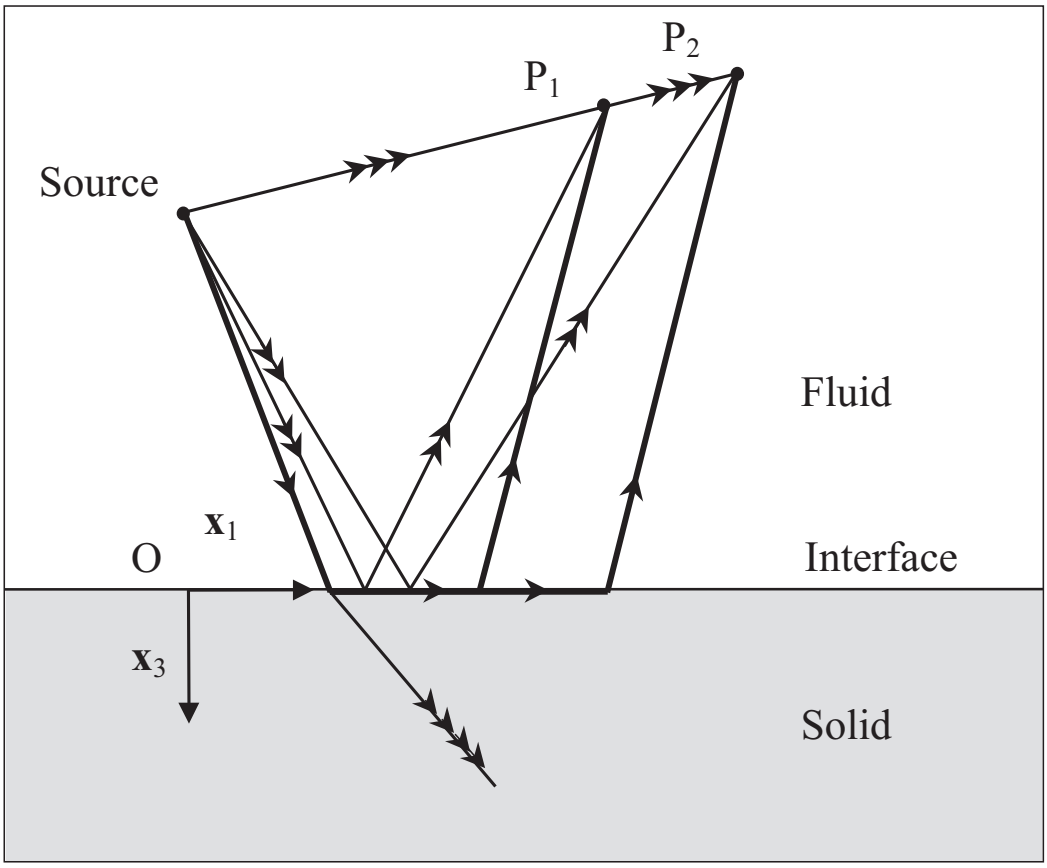

Figure 2.

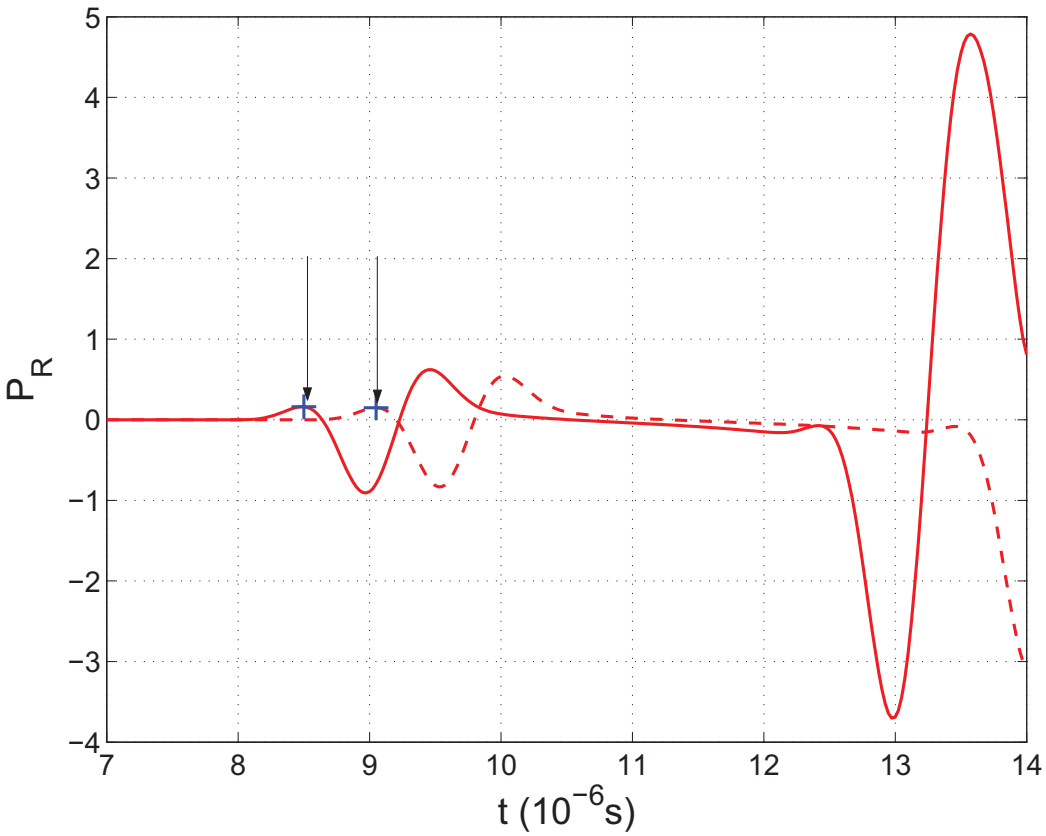

Figure 3.

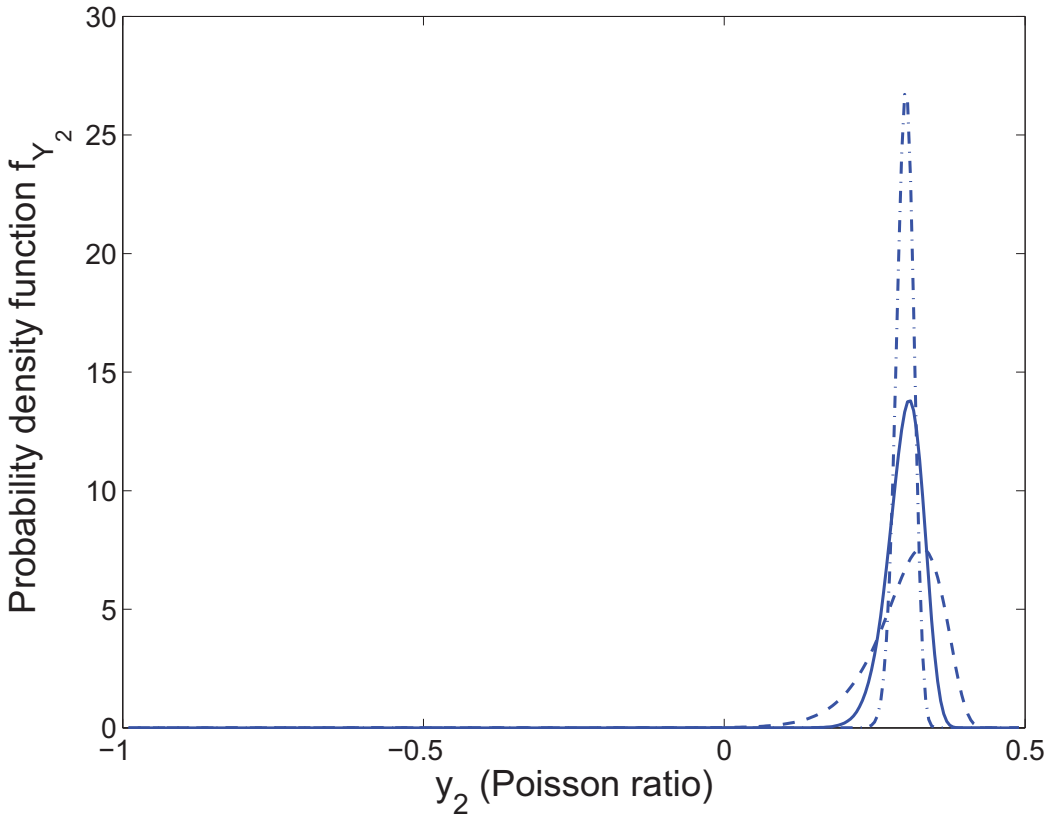
Probability density function f_{Y_2}
30
25
20
15
10
5
0
−1
−0.5
0
0.5
y_2 (Poisson ratio)

Figure 4.

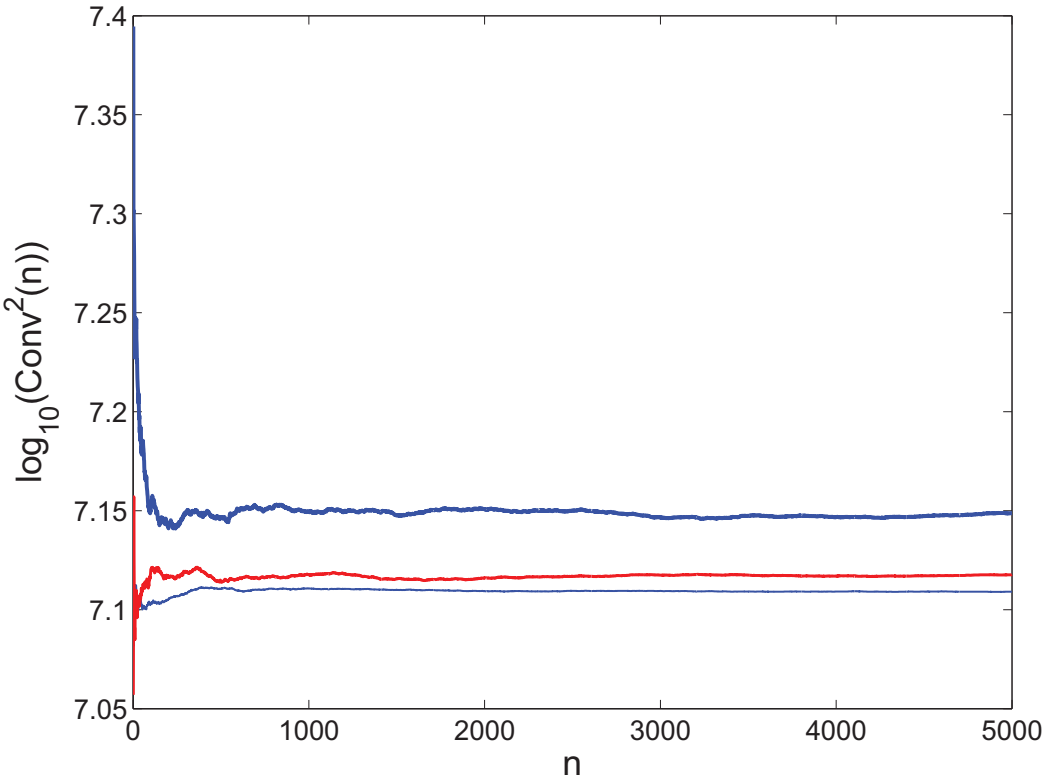
7.4
7.35
7.3
7.25
7.2
7.15
7.1
7.05
0
1000
2000
3000
4000
5000
n
log10(Conv2(n))

Figure 5.

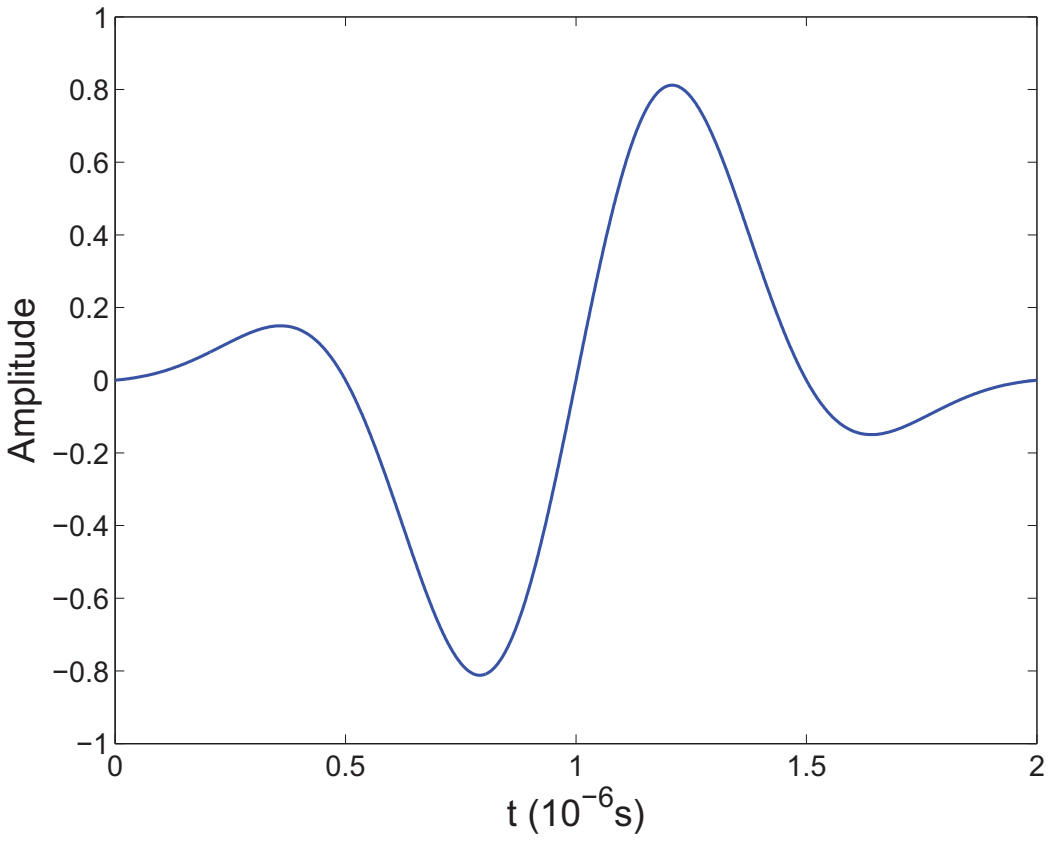

Figure 6.

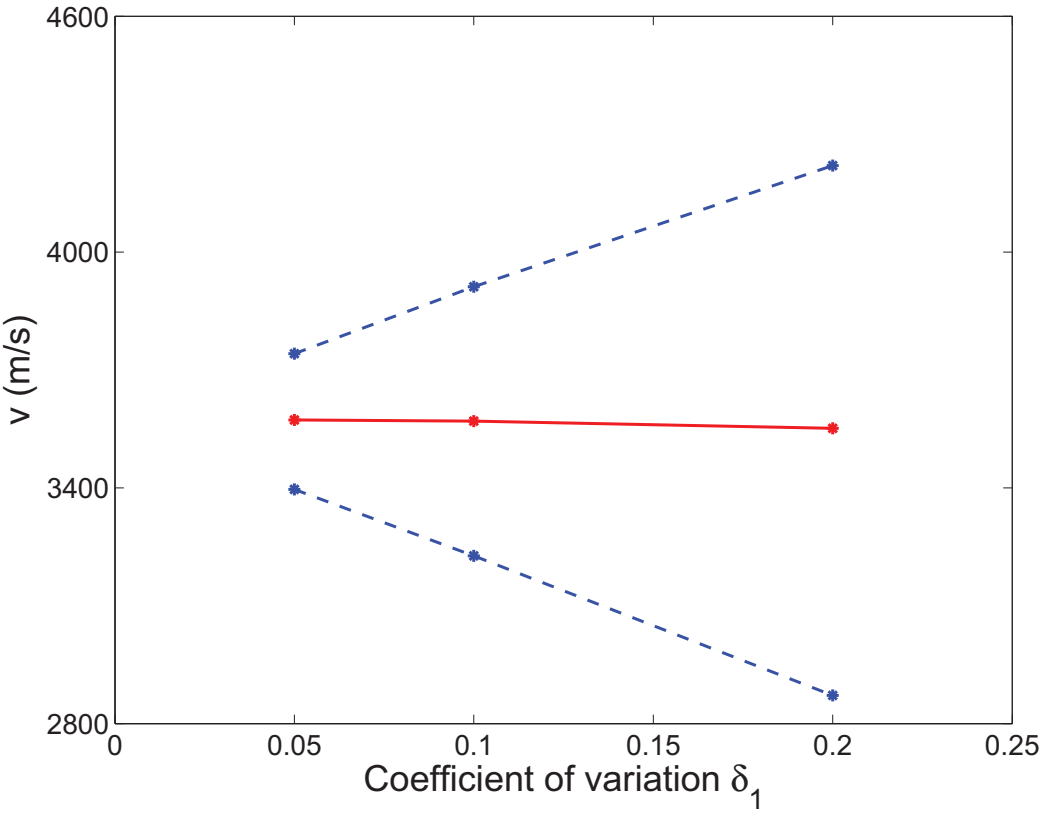
4600
4000
3400
2800
v (m/s)
0
0.05
0.1
0.15
0.2
0.25
Coefficient of variation δ_1

Figure 7.

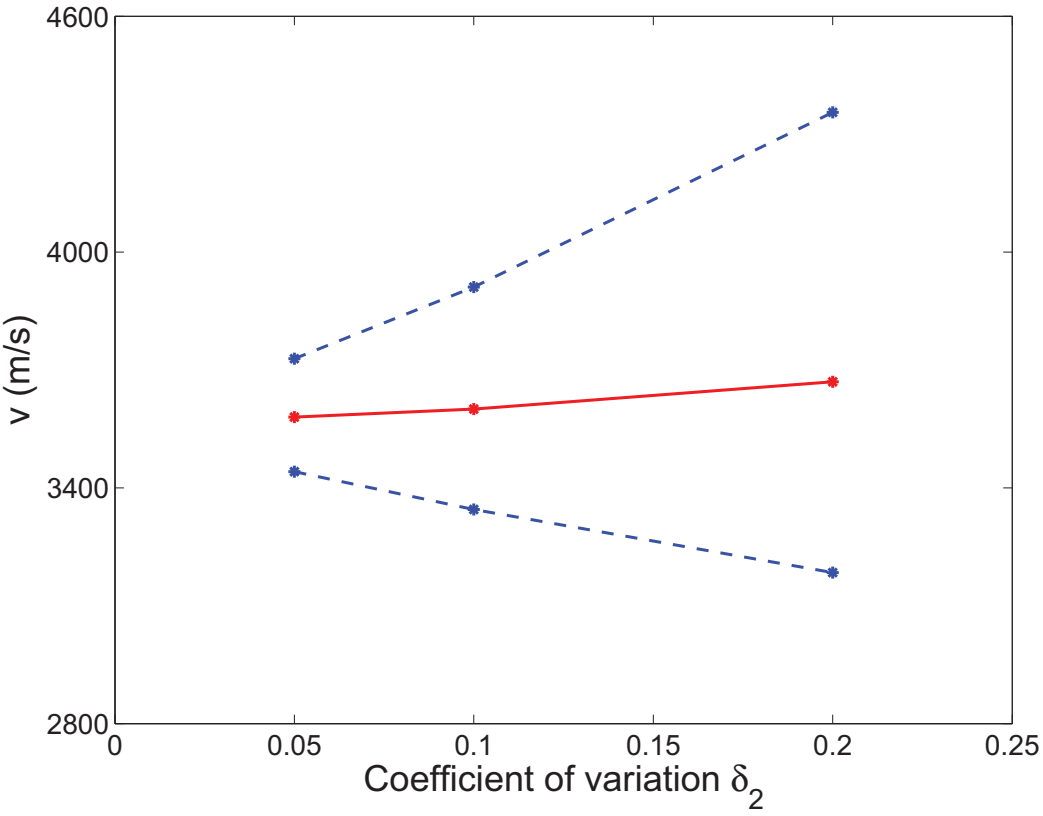
4600
4000
3400
2800
v (m/s)
0
0.05
0.1
0.15
0.2
0.25
Coefficient of variation δ2

Figure 8.

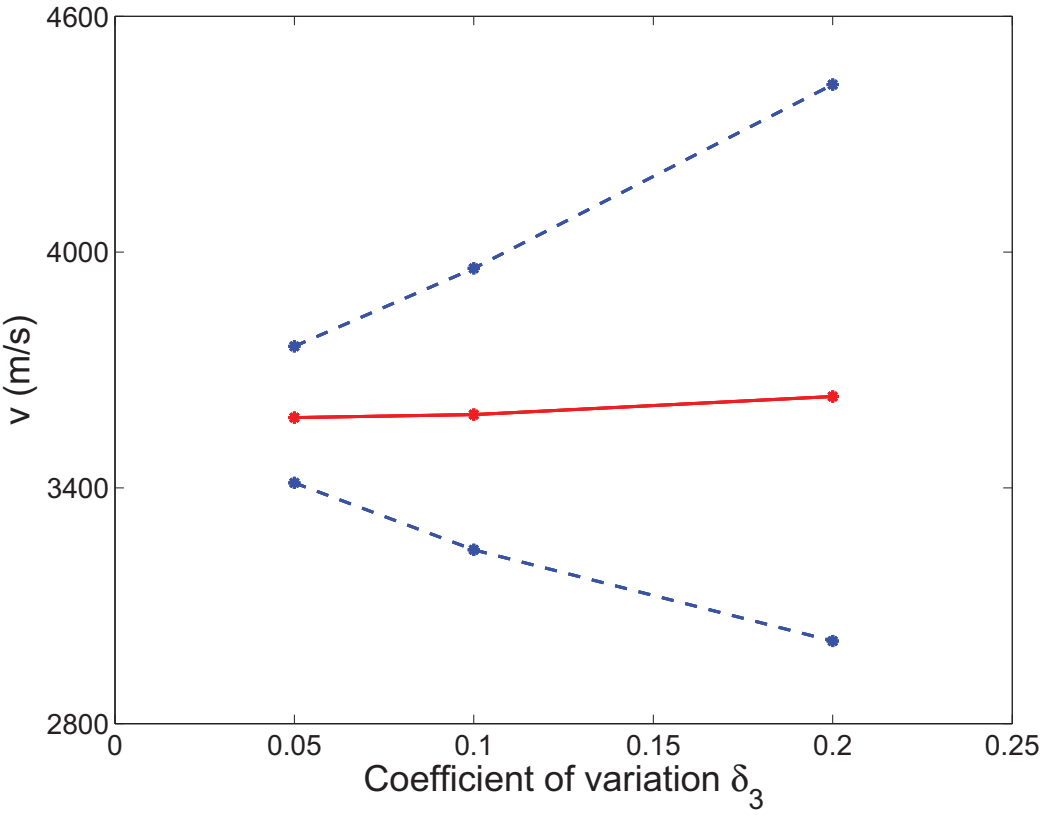
4600
4000
3400
2800
v (m/s)
0
0.05
0.1
0.15
0.2
0.25
Coefficient of variation δ3

Figure 9.

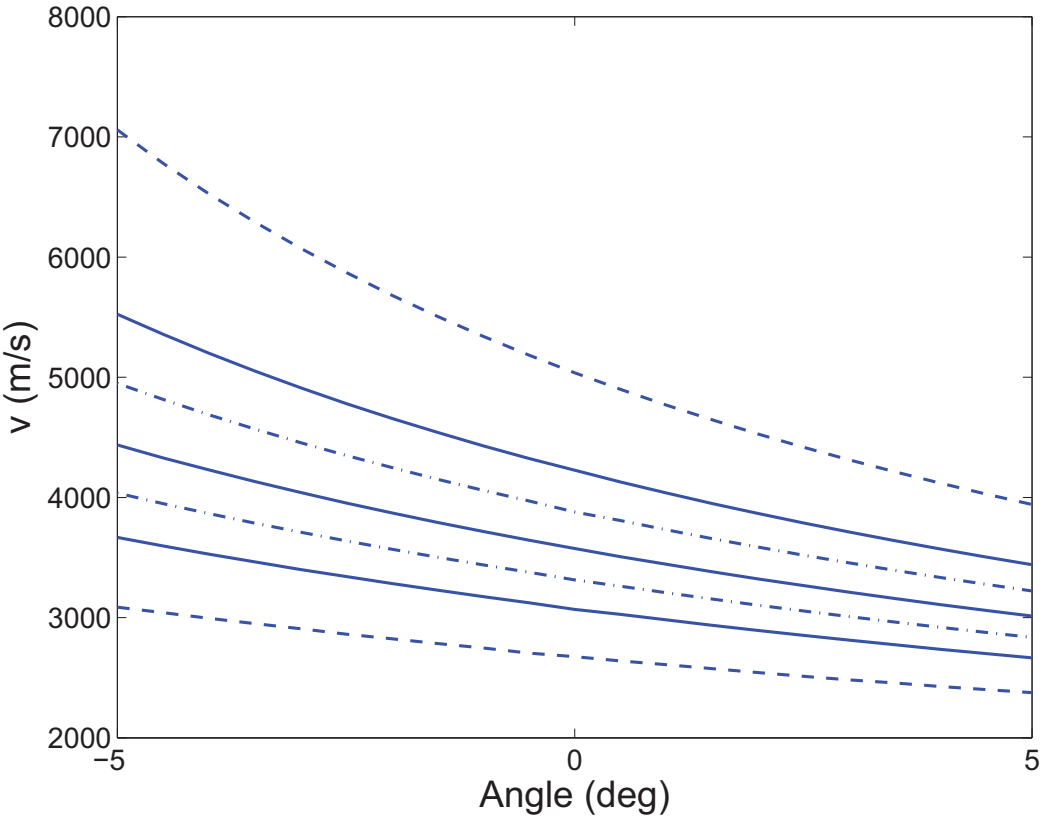

Figure 10.